

## TREND ANALYSIS OF RAIL CORRUGATION IN METRO LINES CONSIDERING FRICTION MEMORY AND INTERFACE EFFECTS

ZHIQIANG WANG, ZHENYU LEI

*Institute of Rail Transit, Tongji University, Shanghai, China*

*e-mail: wangzq@tongji.edu.cn*

In order to investigate the evolution trend of rail corrugation under the action of slip and interface effects, stick-slip vibration characteristics of a wheel-rail system in different line conditions have been analyzed in detail by establishing a complete three-dimensional coupling metro vehicle-track numerical model and considering the friction memory effect characterizing the slip rate and state dependence as well as interface effect. The results show that on a straight line, the friction memory effect has less influence on the wheel-rail contact stick-slip characteristics, and the values and variation ranges of adhesion coefficients and creepages are relatively small, indicating that it is difficult for the wheel-rail system to have stick-slip vibration, which makes it less likely to form rail corrugation. On a curved line, the fluctuation amplitudes of the inside longitudinal stick-slip characteristics and the outside transverse stick-slip characteristics are relatively large, which illustrates that the inside wheel-rail system is more prone to stick-slip vibration in the longitudinal direction, while the outside wheel-rail system is more prone to stick-slip vibration in the transverse direction, thus leading to different forms of rail corrugation. The friction memory effect reduces longitudinal and transverse creepages of both the inside and outside wheel-rail systems, demonstrating that the friction memory effect can moderate the relative wheel-rail slip and thus reduce the development rate of rail corrugation. The interface effect makes longitudinal and transverse adhesion coefficients of the wheel-rail system tend to homogenize and mostly decrease, while the corresponding creepages tend to increase. Although an increase in the creepage induces an enhanced interface slip, a smaller adhesion coefficient does not cause a significant change in the corrugation evolution. Friction memory and interface effects can cause the wheel-rail contact adhesion area ratio to increase, thus making the contact stick-slip distribution tend to homogenize, which is beneficial to reduce wear in the contact area and promote wear to homogenize.

*Keywords:* metro, rail corrugation, friction memory, interface layer, stick-slip characteristics

### 1. Introduction

Rail corrugation, as a structural damage, is prevalent in railway systems around the world, especially in metro lines. Unlike uniform wear of a rail surface material, rail corrugation has periodic characteristics and shows wavy wear along the longitudinal running surface of the rail (Sato *et al.* 2002). Rail corrugation involves both friction and vibration mechanisms of action, where friction determines its damage mechanism, while vibration determines its dynamic mechanism. The existence of rail corrugation will cause abnormal vibration and high-frequency noise of wheel-rail systems, which will easily lead to fatigue damage of vehicle/track components. Therefore, how to effectively prevent and control rail corrugation has become a major problem facing the current railway sector. The wheel-rail contact interface is subject to complex forces and a variety of forms of action, and all variable factors related to it have become the starting point for the study of rail corrugation. It is worth to mention that the formation of rail corrugation is not a single theoretical mechanism (Grassie and Kalousek 1993). Understanding the mechanism

of rail corrugation and exploring its evolution are important prerequisites for achieving effective management of rail corrugation.

Rail corrugation occurs in the contact patch area, and the wheel-rail contact behavior is closely related, so it is more intuitive to study the rail corrugation phenomenon from the micro contact perspective. The stick-slip theory suggests that unstable stick-slip vibration in the wheel-rail contact area contributes to formation and development of rail corrugation. Based on the above theory, Daniel *et al.* (2008) concluded through numerical simulations that the wheel-rail stick-slip had an effect on both long-wavelength and short-wavelength corrugations, and wear was mainly caused by transverse stick-slip vibration. Matsumoto *et al.* (2002), based on experimental and computational results, found that rail corrugation on a curved track was due to stick-slip vibration between the wheel and rail, which was associated with large creepages and vertical force fluctuations. Sun and Simson (2007, 2008) analyzed the effects of curve track parameters, wheel-rail friction characteristics and wheel/rail profile on the stick-slip process, and obtained that the fundamental frequency of the stick-slip process matched the passing frequency of the sleeper and a combined frequency of wheelset torsional and bending vibration. Yao *et al.* (2018) investigated the mechanism of generation of rail corrugation and proposed a micro wavelength-locked extension mechanism of corrugation. The initial stick-slip vibration will lead to formation of initial unevenness on the contact surface, i.e., the initial corrugation, and the evolution of it into the final corrugation also needs to satisfy the phase synchronization condition of stick-slip vibration. The literature (Yang and Li, 2019; Jin *et al.*, 2004; Wen and Jin, 2005) showed that rail surface defects, such as cracks, scratches, transverse geometric defects, etc., were able to ensure the same phase vibration of the stick-slip process, such that rail corrugation was eventually formed. In addition (Eadie *et al.*, 2002; Wang and Lei, 2021, 2022; Shen *et al.*, 2011; Guo *et al.*, 2009) also analyzed the formation process of rail corrugation in terms of contact stick-slip, and combined with field data to verify the correctness of the calculation results.

Most of the current papers using the stick-slip theory to explain corrugation characteristics consider the wheel-rail interface friction property as a constant value, which is not consistent with the variable friction situation in the actual wheel-rail contact due to the slip rate, state and third-body medium. In view of this, this paper focuses on stick-slip characteristics of wheel-rail contact in the presence of slip and interface effects, and analyzes the evolution trend of rail corrugation based on the stick-slip characteristics. Firstly, a three-dimensional coupling metro vehicle-track numerical model in different line conditions is established and the validity of the model is verified by combining the measured data. Then, the friction memory effect is introduced to characterize the slip rate and state dependent friction, and the corresponding contact stick-slip vibration characteristics and their influence on the corrugation trend are analyzed. Finally, on the basis of simultaneous consideration of the friction memory effect and interface effect, the joint action mechanism of both on the stick-slip characteristics and corrugation evolution is investigated in order to further improve the theoretical framework of stick-slip vibration of rail corrugation.

## 2. Numerical model

### 2.1. Establishment of model

Since this paper is mainly concerned with the evolution trend of rail corrugation in metro lines, a vehicle-track three-dimensional coupling numerical model applicable to metro scenarios is established by using the software Universal Mechanism, including the vehicle model, track model and wheel-rail contact model. The vehicle model consists of one vehicle body, two bogies and four wheelsets with the LM wear wheel profile, where the vehicle body and bogies as well as bogies and wheelsets are connected by spring-damping elements to simulate the secondary

and primary suspension. The vehicle body, bogies and wheelsets are all regarded as rigid bodies with 6 degrees of freedom, and the whole vehicle model has 42 degrees of freedom in total. The main structural parameters of the vehicle model are described in (Lei and Wang, 2021; Lei *et al.*, 2019). The rail type in the track model is CHN60, and a Timoshenko beam is used for simulation. The fastener is simulated by the spring-damping element; the track slab (under-rail structure) is built by the finite element method and imported into the track model and then connected to the rail and foundation by the spring-damping element. The main structural parameters of the track model are described in (Li, 2012; Lei and Wang, 2020). The wheel-rail contact model uses a modified CONTACT algorithm, which is based on the Duvaut-Lions variational principle and transforms the friction rolling contact problem into a variational inequality, so as to solve directly for the minimum residual energy expressed by the product of the force acting on the contact patch and displacement (Kalker, 1990; Jin and Xue, 1997). Meantime, the concept of friction memory is introduced in the CONTACT algorithm, which assumes that friction takes time to adapt to a new state and, therefore, there is a memory of the previous state (Vollebregt, 2014). By considering the friction memory of the previous state, the friction coefficient in the contact model is gradually normalized, and the slip rate dependence of friction is characterized through the friction law  $\mu(S)$ . The friction law  $\mu(S)$  is distinguished from the actual friction coefficient  $\mu(x)$ , and the actual friction coefficient  $\mu(x)$  is considered to be proportional to  $\mu(x) - \mu(S)$  and the slip rate  $S$ , as shown below

$$\frac{d\mu}{dx} = -\frac{\max(S(x), S_{min})}{d_c(-V)}[\mu(x) - \mu(S(x))] \quad (2.1)$$

where  $d_c$  is the characteristic slip distance when convergence of the friction coefficient occurs,  $V$  is the vehicle running speed,  $S_{min}$  is the minimum slip rate that allows the friction coefficient to adapt in the adhesion area. It should be mentioned that the implementation of an instantaneous velocity-dependent falling friction law usually leads to numerical instabilities, and the latter can be prevented by the introduction of the mechanism of friction memory (Vollebregt *et al.*, 2021). A schematic diagram of the completed vehicle-track three-dimensional coupling numerical model is shown in Fig. 1.

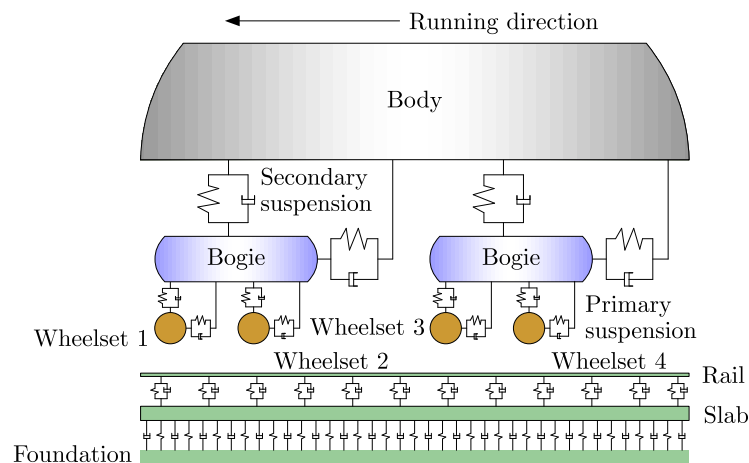


Fig. 1. Diagram of numerical model

## 2.2. Validation of the model

The validity of the numerical model is verified in this Section by using the measured data of rail vertical vibration acceleration of the line interval. For the test process, two sensors are arranged on a section of the measuring point, respectively on both sides of the top surface of the inner rail bottom. The INV3060S instrument is used for data acquisition, the data sampling

frequency is 2048 Hz, the speed is 56 km/h, and the software DASP-V10 is used for data analysis. The layout picture of measuring points in the field test is shown in Fig. 2. For the simulation



Fig. 2. Layout picture of measuring points

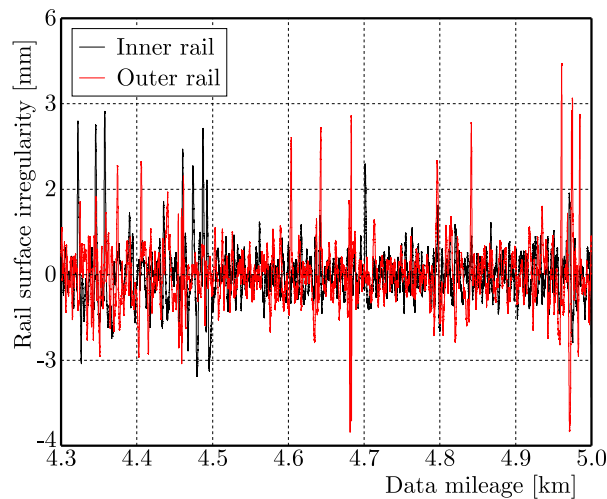


Fig. 3. Rail surface irregularities

process, firstly, the CAT (Corruption Analysis Trolley) acquisition instrument is used to measure the rail surface irregularity in the line interval, as shown in Fig. 3. Then, the measured rail surface irregularity is added to the surface of the rail model and calculation is performed. The vehicle speed in the model is taken as 56 km/h with reference to the current situation, and the rail measurement point is located on the top surface of the inner rail bottom near the track centerline side. The calculated and measured time-frequency domain results of the vertical vibration acceleration of the rail at the measurement point section are shown in Fig. 4. It can be seen that the calculated results are in good agreement with the measured results and meet engineering accuracy requirements, thus verifying validity of the numerical model.

### 3. Wheel-rail contact stick-slip characteristics – considering the friction memory effect

Setting  $d_c$  in Eq. (2.1) of the friction memory effect to 0.01 mm and  $S_{min}$  to 1mm/s, the friction law adopts exponentially decreasing friction, as shown in Fig. 5 (Vollebregt, 2014). By applying the numerical model and performing calculations, the longitudinal and transverse creep

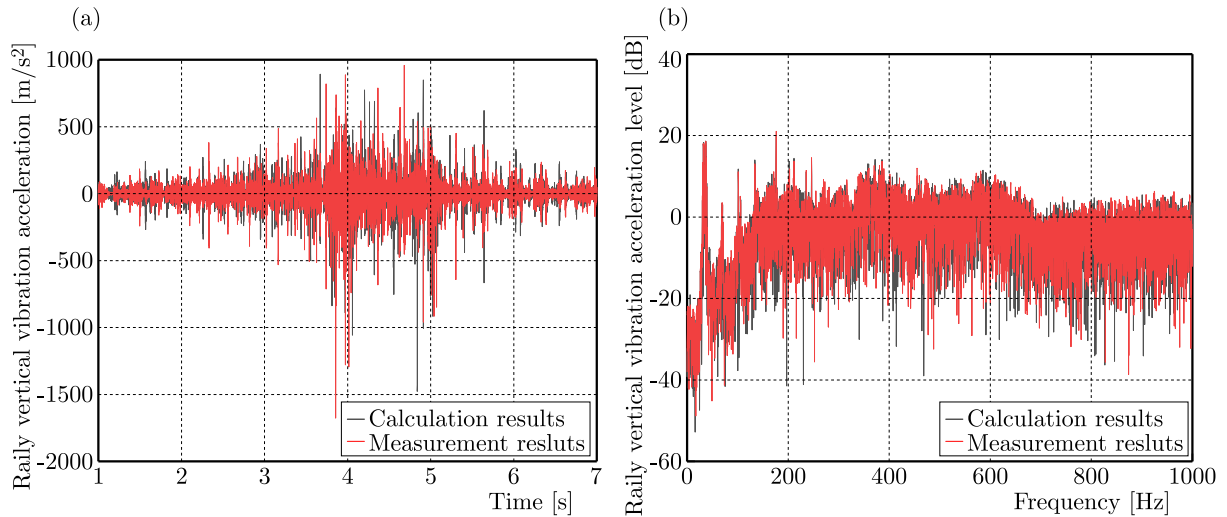


Fig. 4. Results of calculation and measurement: (a) time domain results, (b) frequency domain results

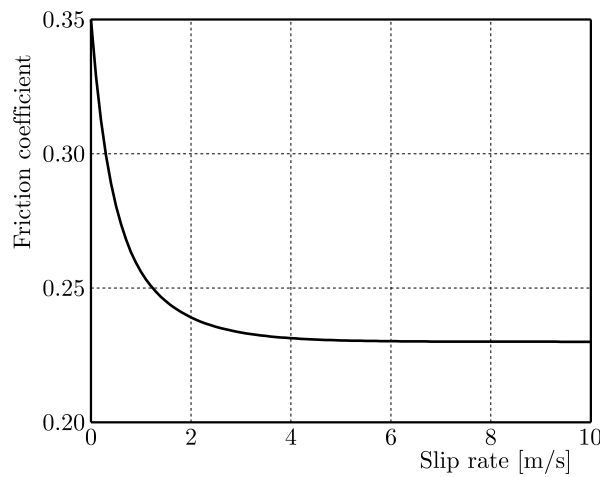


Fig. 5. Curve of the friction coefficient

forces/creepages, normal force and other parameters can be obtained during the operation of the vehicle. The creep force is compared with the normal force as shown in Eq. (3.1) to obtain the wheel-rail interface adhesion coefficient. This paper mainly focuses on the evolution trend of rail corrugation under different conditions by analyzing the relationship between the adhesion coefficient and creepage

$$\alpha_1 = \frac{F_1}{P_3} \quad \alpha_2 = \frac{F_2}{P_3} \quad (3.1)$$

where  $\alpha_1$  and  $\alpha_2$  are longitudinal and transverse adhesion coefficients,  $F_1$  and  $F_2$  are longitudinal and transverse creep forces,  $P_3$  is the normal force.

### 3.1. Straight line condition

In this Section, stick-slip characteristics of wheel-rail contact for the straight line condition are analyzed, and scatter diagrams of calculated longitudinal and transverse stick-slip characteristics after introducing the friction memory effect are shown in Fig. 6. As a comparison, the scatter diagrams of longitudinal and transverse stick-slip characteristics without considering the friction memory effect are shown in Fig. 7. To eliminate the influence of surface irregularities

and defects on calculation results, both the rail and wheel surfaces in the model are smooth, standard type surfaces (the same below). The vehicle speed in the model is 56 km/h and the static friction coefficient of wheel-rail contact is 0.35.

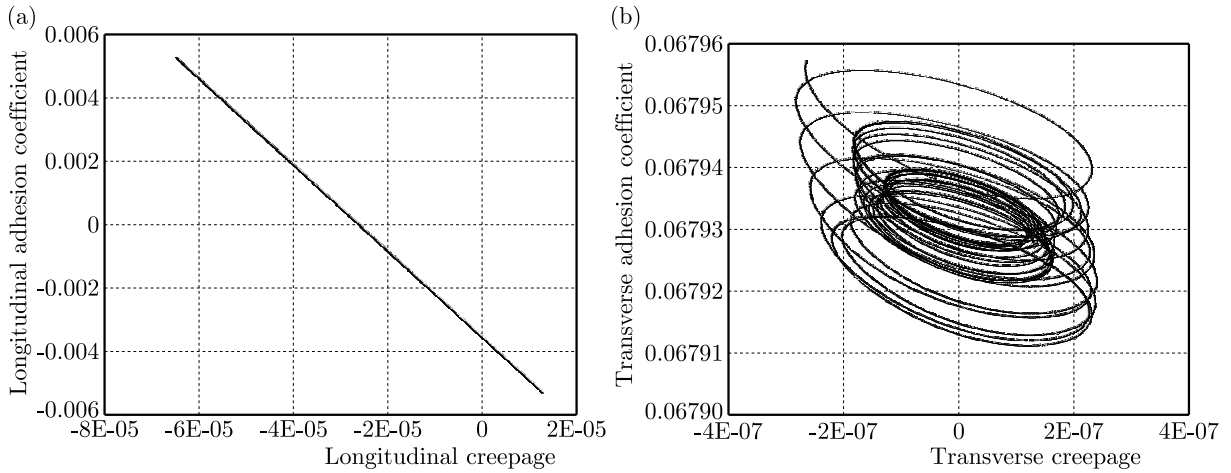


Fig. 6. Diagrams of wheel-rail contact stick-slip characteristics – straight line condition with considering the friction memory effect: (a) longitudinal stick-slip characteristics, (b) transverse stick-slip characteristics

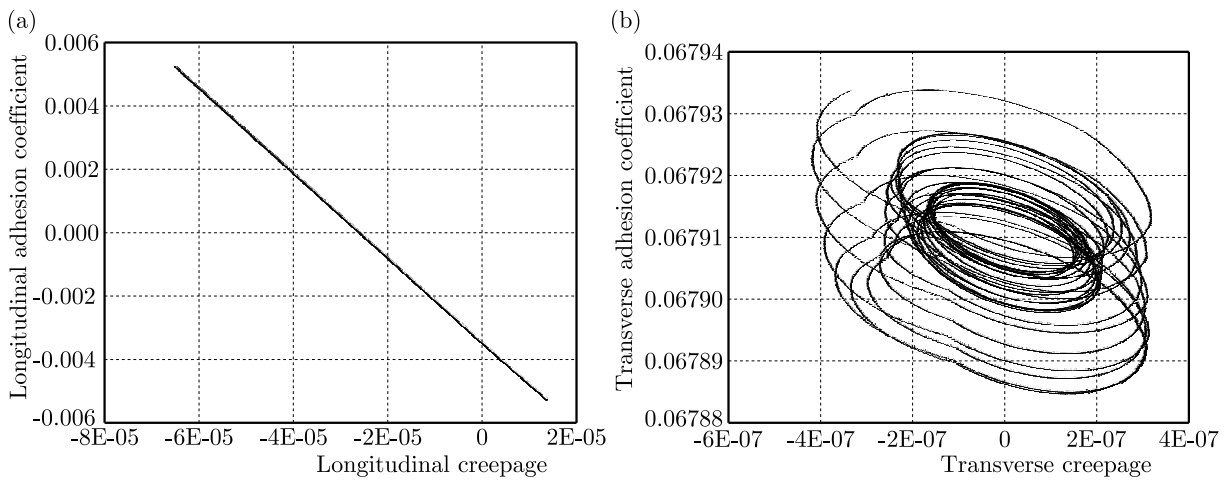


Fig. 7. Diagrams of wheel-rail contact stick-slip characteristics – straight line condition without considering the friction memory effect: (a) longitudinal stick-slip characteristics, (b) transverse stick-slip characteristics

By comparing Figs. 6 and 7, it is easy to find that the longitudinal and transverse stick-slip characteristic diagrams are similar in both cases, indicating that the introduction of the friction memory effect has a small effect on the stick-slip characteristics of wheel-rail contact on a straight line. The longitudinal adhesion coefficient shows a linear relationship with longitudinal creepage, while the transverse adhesion coefficient shows a spiral fluctuation relationship with transverse creepage, which is related to hunting motion of the wheelset. In general, for the straight line condition, the longitudinal/transverse adhesion coefficients and longitudinal/transverse creepages are small, and the corresponding variation ranges are also small, which shows that under the condition of a smooth contact interface, the stick-slip vibration is difficult to occur on the straight line, so it is not easy to induce corrugation.

### 3.2. Curve line condition

The scatter diagrams of wheel-rail contact stick-slip characteristics on a curved line with and without the friction memory effect are shown in Figs. 8 and 9. In the model, the track line type is a circular curve, the curve radius is 350 m, the outer rail superelevation is 105 mm, the gauge is 1435 mm, and other conditions are the same as those in the straight line condition.

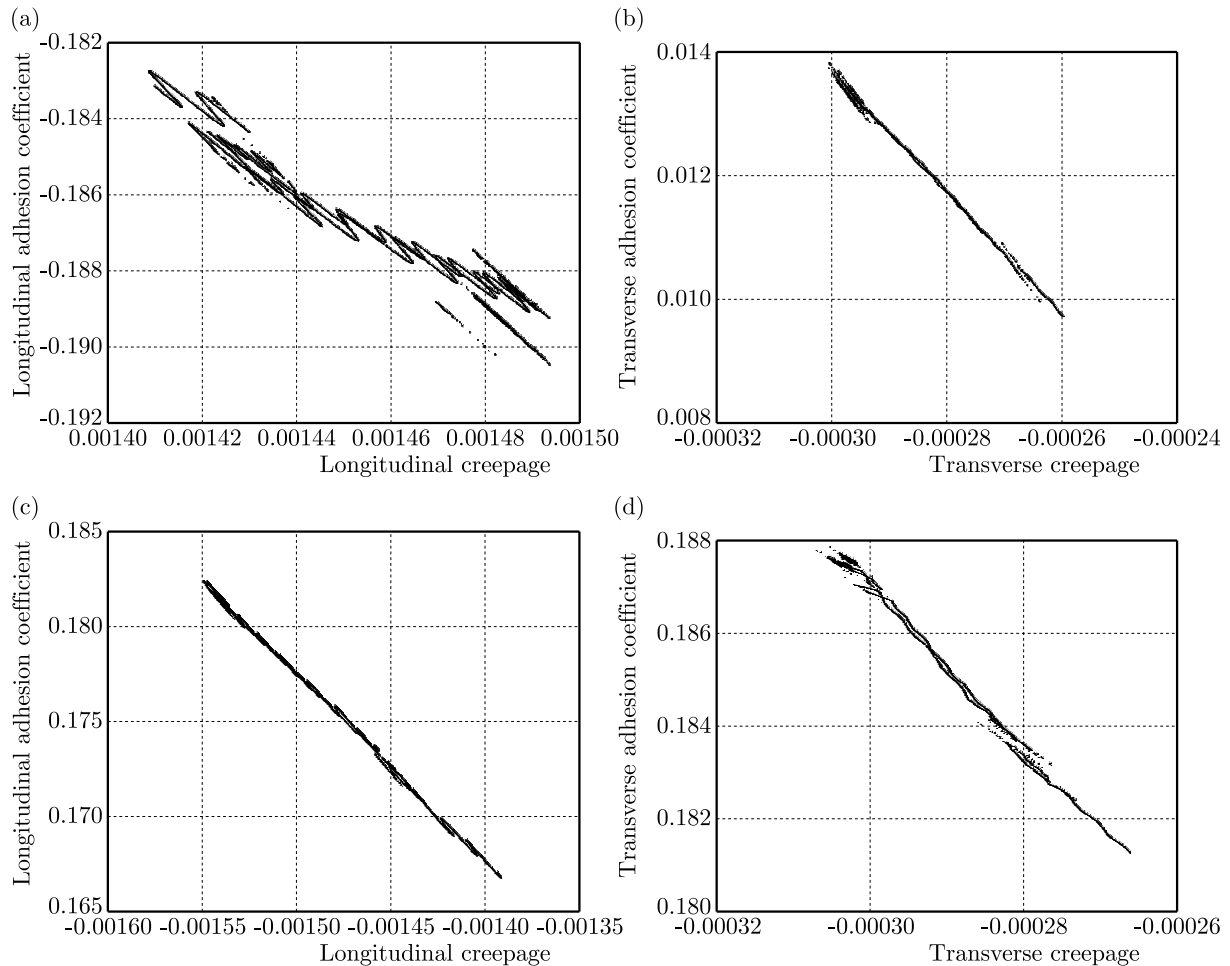


Fig. 8. Diagrams of wheel-rail contact stick-slip characteristics – curved line condition with considering the friction memory effect: (a) inside longitudinal stick-slip characteristics, (b) inside transverse stick-slip characteristics, (c) outside longitudinal stick-slip characteristics, (d) outside transverse stick-slip characteristics

From Figs. 8 and 9, it can be obtained that the longitudinal and transverse adhesion coefficients of both inside and outside wheel-rail systems are almost linearly related to the corresponding creepages on the curve line. The fluctuation amplitudes of the scatter diagram of the longitudinal stick-slip characteristics of the inner side and the transverse stick-slip characteristics of the outer side are relatively large, which indicates that the inside wheel-rail system is more prone to stick-slip vibration in the longitudinal direction, while the outside wheel-rail system is more prone to stick-slip vibration in the transverse direction, leading to different forms of rail corrugation. By comparing Figs. 8 and 9, it can be seen that after the introduction of the friction memory effect, the longitudinal and transverse creepages of the inside and outside wheel-rail systems are reduced, illustrating that the friction memory effect alleviates the slip phenomenon in the wheel-rail system. Since slip is closely related to material wear (Archard,

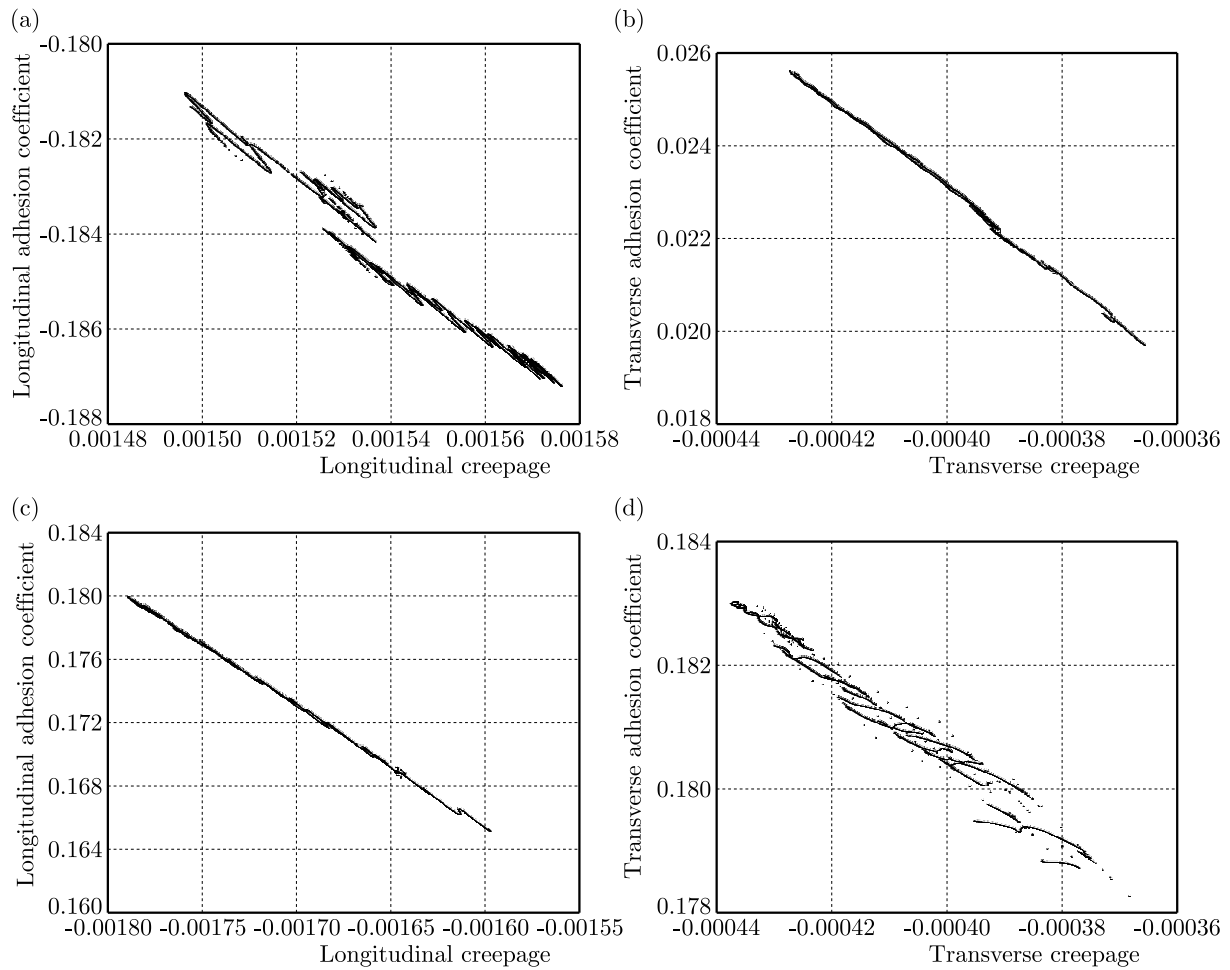


Fig. 9. Diagrams of wheel-rail contact stick-slip characteristics – curved line condition without considering the friction memory effect: a) inside longitudinal stick-slip characteristics, (b) inside transverse stick-slip characteristics, (c) outside longitudinal stick-slip characteristics, (d) outside transverse stick-slip characteristics

1953), the friction memory effect will reduce the development rate of rail corrugation in the wavelength-fixed condition of wear (Grassie, 2009).

#### 4. Wheel-rail contact stick-slip characteristics – considering friction memory and interface effects

Based on the results in Section 3, the wheel-rail contact stick-slip characteristics under the action of the interface layer between the wheel and rail are further considered. Setting the shear modulus of the interface layer to  $8.2 \cdot 10^9$  Pa and thickness to 1.25 mm for simulating an ideal natural third-body layer between the wheel and rail (Berthier *et al.*, 2004; Vollebregt, 2014), the calculated scatter diagrams of the stick-slip characteristics are shown in Figs. 10 and 11.

By comparing Fig. 10 and Fig. 6, it can be obtained that the longitudinal and transverse adhesion coefficients of the wheel-rail system on the straight line are reduced after the introduction of the interface effect, while the corresponding creepages show an increasing trend. Although an increase in the creepage drives enhanced interface slip, a relatively small adhesion coefficient does not lead to significant changes in the evolution trend of rail corrugation. Similarly, by comparing Fig. 11 and Fig. 8, it can be found that the longitudinal and transverse creepages of the

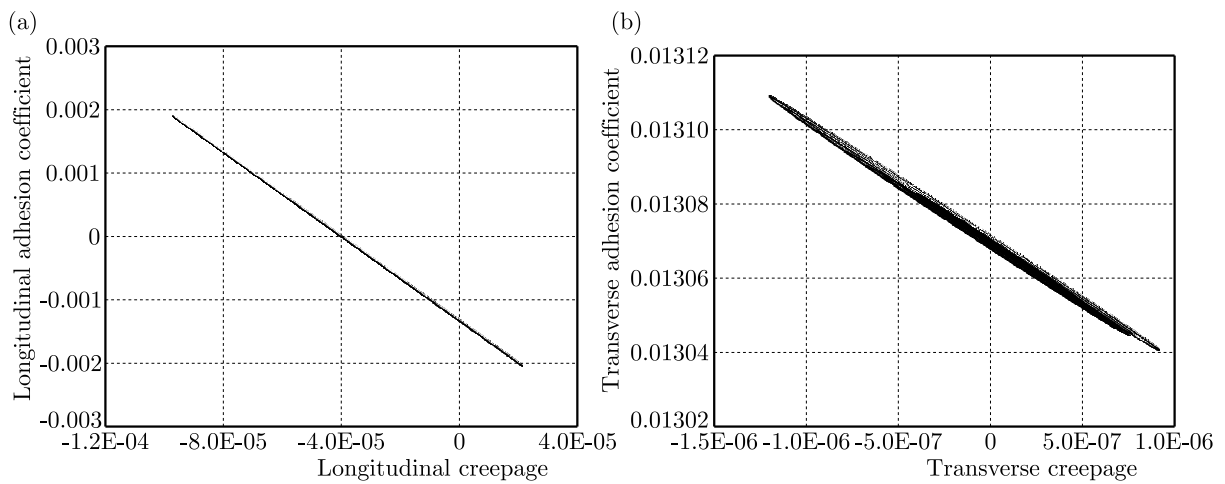


Fig. 10. Diagrams of wheel-rail contact stick-slip characteristics – straight line condition with considering the friction memory and interface effects: (a) longitudinal stick-slip characteristics, (b) transverse stick-slip characteristics

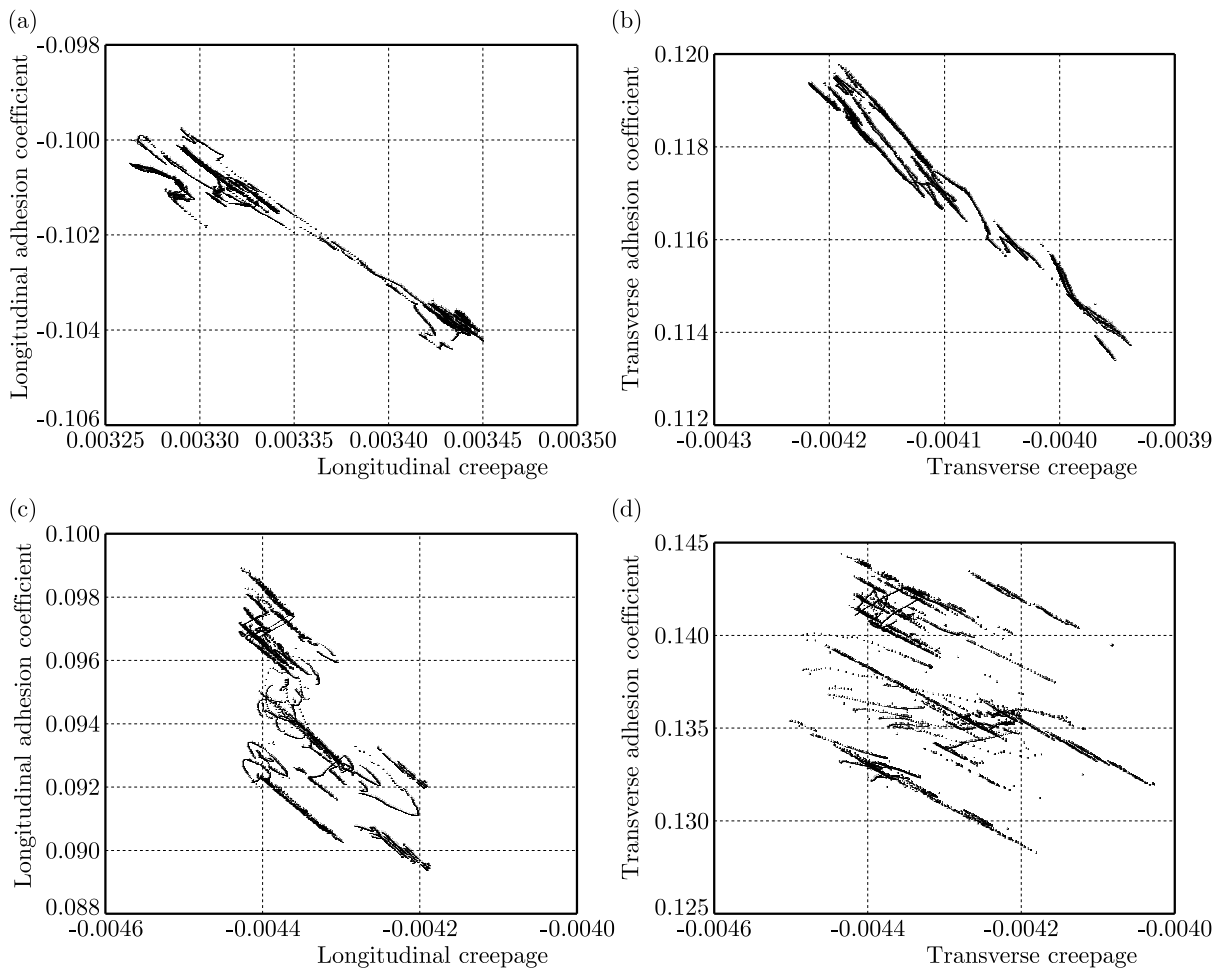


Fig. 11. Diagrams of wheel-rail contact stick-slip characteristics – curved line condition with considering friction memory and interface effects: (a) inside longitudinal stick-slip characteristics, (b) inside transverse stick-slip characteristics, (c) outside longitudinal stick-slip characteristics, (d) outside transverse stick-slip characteristics

inside and outside wheel-rail systems generally increase, while the corresponding adhesion coefficients, except for the transverse adhesion coefficient of the inside wheel-rail system, decrease. The reason for this is that the introduction of the interface layer makes the longitudinal and transverse adhesion coefficients tend to be homogeneous (around 0.100), which can also be seen from the degree of dispersion of the scattered points in Fig. 11.

In addition, by comparing Fig. 10b and Fig. 6b, it is easy to see that the adhesion coefficients are more concentrated after introducing the interface effect, which may be related to the stick-slip distribution in the contact area. In order to clarify the cause of the above phenomenon, the adhesion area ratios in the contact patch considering only the friction memory effect, friction memory and interface effects, and without any effect are respectively calculated, as shown in Fig. 12. According to Fig. 12a, when considering friction memory and interface effects, the adhesion area ratio tends to be close to 1, which is much higher than the other two cases, demonstrating that the whole contact patch is almost adhesive. The distribution form is relatively simple, and this may be the main reason why Fig. 10b is different from Fig. 6b. Meantime, it can also be seen from Fig. 12b that the introduction of friction memory and interface effects will increase the adhesion area ratio, so that the contact stick-slip distribution tends to be uniform, which will reduce wear in the contact patch and promote it to be uniform. Furthermore, in the curved line condition, it is easy to see that there are some jumpy transitions in the contact area, and the degree of jumpy transitions in the contact area of the outer rail is significantly larger than that of the inner rail (especially when friction memory and interface effects are considered at the same time). This is related to frequent side contact between the outer wheel flange and the outer rail gauge for a small radius curve.

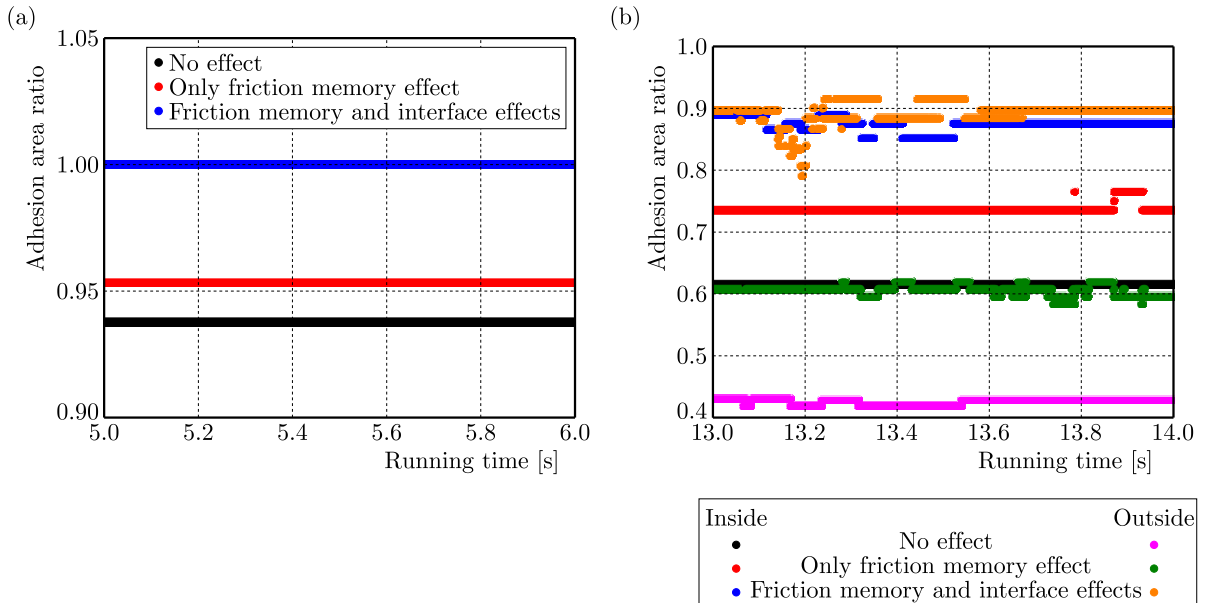


Fig. 12. Diagrams of wheel-rail contact adhesion area ratios: (a) straight line condition, (b) curved line condition

## 5. Conclusions

By establishing a three-dimensional coupling numerical model of a metro vehicle-track system under different line conditions, and considering the friction memory effect characterizing the slip rate and state dependence as well as the interface effect, this paper analyzes stick-slip vibration characteristics of the wheel-rail system and the evolution trend of rail corrugation in detail. The main conclusions are as follows:

- On a straight line, the introduction of the friction memory effect has little impact on a stick-slip characteristics of wheel-rail contact, and values and variation ranges of adhesion coefficients and creepages are relatively small, which indicates that the wheel-rail system is difficult to generate stick-slip vibration, and thus it is not easy to produce rail corrugation.
- On a curved line, fluctuation amplitudes of the inside longitudinal stick-slip characteristics and outside transverse stick-slip characteristics are relatively large, which illustrates that the inside wheel-rail system is more prone to stick-slip vibration in the longitudinal direction, while the outside wheel-rail system is more prone to stick-slip vibration in the transverse direction, thus leading to different forms of rail corrugation. The introduction of the friction memory effect reduces longitudinal and transverse creepages of both the inside and outside wheel-rail systems, demonstrating that the friction memory effect alleviates the slip phenomenon, thereby reduces the development rate of rail corrugation.
- The introduction of the interface effect leads to homogenization of longitudinal and transverse adhesion coefficients of the wheel-rail system and most of them show a decreasing trend, while the corresponding creepages show an increasing trend. Although the increase of the creepage will enhance the interface slip, the smaller adhesion coefficient will not cause significant changes in the corrugation evolution.
- The introduction of friction memory and interface effects will increase the adhesion area ratio in the wheel-rail contact patch, thus making the contact stick-slip distribution tend to be uniform, which will reduce wear in the contact patch and promote it to be uniform.

## References

1. ARCHARD J.F., 1953, Contact and rubbing of flat surfaces, *Journal of Applied Physics*, **24**, 8, 981-988
2. BERTHIER Y., DESCARTES S., BUSQUET M., NICCOLINI E., DESRAYAUD C., BAILLET L., BAIETTO-DUBOURG M.C., 2004, The role and effects of the third body in the wheel-rail interaction, *Fatigue and Fracture of Engineering Materials and Structures*, **27**, 5, 423-436
3. DANIEL W.J.T., HORWOOD R.J., MEEHAN P.A., WHEATLEY N., 2008, Analysis of rail corrugation in cornering, *Wear*, **265**, 9-10, 1183-1192
4. EADIE D.T., KALOUSEK J., CHIDDICK K.C., 2002, The role of high positive friction (HPF) modifier in the control of short pitch corrugations and related phenomena, *Wear*, **253**, 1-2, 185-192
5. GRASSIE S.L., 2009, Rail corrugation: characteristics, causes, and treatments, *Proceedings of the Institution of Mechanical Engineers Part F-Journal of Rail and Rapid Transit*, **223**, 6, 581-596
6. GRASSIE S.L., KALOUSEK J., 1993, Rail corrugation: characteristics, causes and treatments, *Proceedings of the Institution of Mechanical Engineers, Part F: Journal of Rail and Rapid Transit*, **207**, 1, 57-68
7. GUO M.H., ZHANG X.H., SHEN G., 2009, Study on rail corrugation mechanism in curved track of metro, *Modern Urban Transit*, **4**, 60-62+1
8. JIN X.S., WEN Z.F., WANG K.Y., ZHANG W.H., 2004, Effect of a scratch on curved rail on initiation and evolution of rail corrugation, *Tribology International*, **37**, 5, 385-394
9. JIN X.S., XUE B.Y., 1997, Application of three-dimensional non-Hertzian rolling contact theory to wheel/rail interactions – compilation and application of TPLR, *Journal of Southwest Jiaotong University*, **32**, 4, 53-58
10. KALKER J.J., 1990, *Three-Dimensional Elastic Bodies in Rolling Contact*, Vol. 2, Springer Science & Business Media
11. LEI Z.Y., WANG Z.Q., 2020, Generation mechanism and development characteristics of rail corrugation of Cologne egg fastener track in metro, *KSCE Journal of Civil Engineering*, **24**, 6, 1763-1774

12. LEI Z.Y., WANG Z.Q., 2021, Contact and creep characteristics of wheel-rail system under harmonic corrugation excitation, *Journal of Vibration and Control*, **27**, 17-18, 2069-2080
13. LEI Z.Y., WANG Z.Q., LI L., GENG C.Z., 2019, Rail corrugation characteristics of the common fastener track in metro, *Journal of Tongji University (Natural Science)*, **47**, 9, 1334-1340
14. LI X., 2012, *Study on the Mechanism of Rail Corrugation on Subway Track*, Southwest Jiaotong University, Chengdu
15. MATSUMOTO A., SATO Y., ONO H., TANIMOTO M., OKA Y., MIYAUCHI E., 2002, Formation mechanism and countermeasures of rail corrugation on curved track, *Wear*, **253**, 1-2, 178-184
16. SATO Y., MATSUMOTO A., KNOTHE K., 2002, Review on rail corrugation studies, *Wear*, **253**, 1-2, 130-139
17. SHEN G., ZHANG X.H., GUO M.H., 2011, Theoretical study on rail corrugation on curved track of metro systems, *Journal of Tongji University (Natural Science)*, **39**, 3, 381-384
18. SUN Y.Q., SIMSON S., 2007, Nonlinear three-dimensional wagon-track model for the investigation of rail corrugation initiation on curved track, *Vehicle System Dynamics*, **45**, 2, 113-132
19. SUN Y.Q., SIMSON S., 2008, Wagon-track modelling and parametric study on rail corrugation initiation due to wheel stick-slip process on curved track, *Wear*, **265**, 9-10, 1193-1201
20. VOLLEBREGT E.A.H., 2014, Numerical modeling of measured railway creep versus creep-force curves with CONTACT, *Wear*, **314**, 1-2, 87-95
21. VOLLEBREGT E.A.H., SIX K., POLACH O., 2021, Challenges and progress in the understanding and modelling of the wheel-rail creep forces, *Vehicle System Dynamics*, **59**, 7, 1026-1068
22. WANG Z.Q., LEI Z.Y., 2021, Formation mechanism of metro rail corrugation based on wheel-rail stick-slip behaviors, *Applied Sciences-Basel*, **11**, 17, 8128
23. WANG Z.Q., LEI Z.Y., 2022, Formation mechanism of rail corrugation on the small radius curve of metro based on stick-slip torsional vibration, *Journal of Southeast University (Natural Science)*, **52**, 5, 998-111
24. WEN Z.F., JIN X.S., 2005, Effect of track lateral geometry defects on corrugations of curved rails, *Wear*, **259**, SI, 1324-1331
25. YANG Z., LI Z.L., 2019, A numerical study on waves induced by wheel-rail contact, *International Journal of Mechanical Sciences*, **161-162**, 105069
26. YAO H.M., SHEN G., GAO L.J., 2018, Formation mechanism of worn profile rail corrugation based on experimental verification, *Journal of Tongji University (Natural Science)*, **46**, 10, 1427-1432

*Manuscript received December 20, 2022; accepted for print February 9, 2023*